Title: Quantifying intracellular protein binding thermodynamics during mechanotransduction based on FRET spectroscopy.

Authors: Abdul Rahim NA, Pelet S, Mofrad MR, So PT, Kamm RD

Journal: Methods (San Diego, Calif.)

Year: 2014 Mar 15

Volume: 66

Issue: 2

Pages: 208-21

DOI: 10.1016/j.ymeth.2013.10.007

Published in final edited form as:
Methods. 2014 March 15; 66(2): 208–221. doi:10.1016/j.ymeth.2013.10.007.

Quantifying intracellular protein binding thermodynamics during mechanotransduction based on FRET spectroscopy

Nur Aida Abdul Rahim[1], **Serge Pelet**[2,3], **Mohammad R K Mofrad**[4], **Peter T C So**[1,2,5,*], and **Roger D Kamm**[1,2]

[1]Department of Mechanical Engineering, Massachusetts Institute of Technology, 77 Mass Ave, Cambridge, MA 02139 [2]Department of Biological Engineering, Massachusetts Institute of Technology, 77 Mass Ave, Cambridge, MA 02139 [3]Department of Fundamental Microbiology, Biophore Building, Room 2406, University of Lausanne, CH-1015 Lausanne, Switzerland [4]Department of Bioengineering, 306 Stanley Hall MC #1762, University of California Berkeley, Berkeley, CA 94720-1762 [5]Laser Biomedical Research Center, a NIH NIBIB Research Resource, Massachusetts Institute of Technology, 77 Mass Ave, Cambridge, MA 02139

Abstract

Mechanical force modulates myriad cellular functions including migration, alignment, proliferation, and gene transcription. Mechanotransduction, the transmission of mechanical forces and its translation into biochemical signals, may be mediated by force induced protein conformation changes, subsequently modulating protein signaling. For the paxillin and focal adhesion kinase interaction, we demonstrate that force-induced changes in protein complex conformation, dissociation constant, and binding Gibbs free energy can be quantified by lifetime-resolved fluorescence energy transfer microscopy combined with intensity imaging calibrated by fluorescence correlation spectroscopy. Comparison with in vitro data shows that this interaction is allosteric in vivo. Further, spatially resolved imaging and inhibitor assays show that this protein interaction and its mechano-sensitivity are equal in the cytosol and in the focal adhesions complexes indicating that the mechano-sensitivity of this interaction must be mediated by soluble factors but not based on protein tyrosine phosphorylation.

Keywords

FRET; FLIM; FCS; mechanotransduction; paxillin; focal adhesion kinase

*Corresponding author: Peter T. C. So, Department of Mechanical and Biological Engineering, Massachusetts Institute of Technology, NE47-279, 77 Mass Ave, Cambridge, MA 02139, Phone: (617) 253-6552, Fax: (617) 324-7554, ptso@mit.edu.

1. Introduction

Cellular processes such as proliferation, differentiation, and migration are regulated by biochemical signals transduced through protein-protein interactions. In order to study these processes, assays have been developed to quantify the complex signaling network. To detect intracellular protein assembly, there are well-established in vitro assays such as co-immunoprecipitation [1, 2]. More quantitative approaches can further measure protein binding constants in purified protein solutions, including isothermal titration calorimetry (ITC) [3-5], nuclear magnetic resonance (NMR) [6], surface plasmon resonance (SPR) [7-9], and fluorescence correlation spectroscopy (FCS) [10-13]. Given their in vitro nature, the applicability of these methods in understanding dynamic cellular processes is fairly limited. Clearly, the development of quantitative assays that are applicable to track dynamic intracellular processes would be very useful. An important advance is the development of genetically expressible proteins that enable tagging and tracking of proteins with minimal perturbation [14-16]. Within the past decade, FCS and its variants such as fluorescence cross-correlation spectroscopy (FCCS) have been shown to be powerful methods to study protein binding in vivo. Kim et al. utilizes two-photon FCCS to measure binding constants between calmodulin (CaM) and Ca^{2+} / CaM-dependent protein kinase II (CaMKII) under various conditions, in what is probably the first to quantify intracellular binding constant [17]. Subsequently, others have measured intracellular association/dissociation constants of other proteins based using similar approaches [18-20]. In this paper, we report a new approach based on combining Förster or fluorescence resonance energy transfer (FRET) with intensity imaging calibrated by FCS that is able to: (1) determine whether protein binding occurs and the conformation information of the bound protein complex, (2) quantify the fraction of bound and free proteins, (3) measure thermodynamic constants of protein binding such as the dissociation constant and Gibbs free energy. Importantly, this method is relatively fast and allows all these parameters to be measured throughout the cell, producing distribution maps of protein-protein interaction parameters.

FRET can be readily measured by fluorescence lifetime microscopy (FLIM) and is increasingly used to answer questions related to binding of intracellular proteins [21, 22]. Peter and co-workers demonstrated a novel receptor-kinase interaction between the chemokine receptor (CXCR4) and protein kinase C (PKC)α in carcinoma cells using an EGFP-mRFP1 FRET pair [23]. A GFP-Cy3 FRET pair used by Parsons et al. detected activated Cdc42 interacting with PAK1 in a location-dependent manner [24]. Due to the nanometer scale distance over which FRET is relevant, a positive FRET readout detected through changes in donor fluorescence lifetime most likely denotes direct protein interaction. However, most current FRET/FLIM studies stop at the determination of average lifetimes or calculation of interfluorophore distance. It is important to note that FRET also provides information on the ratio of bound to free protein. Combining this information with intensity-concentration measurements calibrated by FCS, it is possible to determine intracellular bound protein distribution and to map dissociation constant and binding free energy of binding for our protein pair of interest within cells.

As a demonstration of quantitative thermodynamic measurement of protein-protein interactions in vitro, we study an aspect of the mechanotransduction process in endothelial

cells. The endothelium experiences mechanical forces in the form of hemodynamic shear stress and pulsatile pressure-induced stretch. While signaling cascades that result from mechanical forces have been extensively characterized [25, 26], the initiating processes for mechanotransduction are still not fully understood. Adherent cells can sense deformation of their substrate where an external mechanical perturbation to the basal membrane is transmitted to the cytoskeleton through integrins and the associated proteins at focal adhesions (FAs). Extensive schematic maps of the more than fifty different proteins associated with FAs are available [27, 28], and many of these have been implicated in mechanotransduction. The quantification of the mechano-sensitivity of the binding affinities of these proteins and the conformations of these molecular complexes would provide valuable insights. In this study, we chose to characterize the interaction between two of these proteins, paxillin (Pax) and focal adhesion kinase (FAK) [29, 30]. Paxillin is a 70 kDa protein with five peptide sequence, LD motifs, close to its N-terminus that are involved with binding to other proteins [31]. Specifically LD2 and LD4 are known to be involved with FAK binding. FAK is an even larger protein of 125 kDa. The FAK domain that directly interacts with Pax is referred to as the focal adhesion targeting sequence (FAT) [32] [33]. FAT is known structurally as a four helix bundle with two hydrophobic sites on its front and back that are involved with Pax binding. Recent advances in FCS and related techniques such as FCCS and N&B analysis have produced a wealth of data in characterizing the binding stoichiometry and diffusion properties of these protein pairs at the FAs and the cytosol [34-38]. Our studies on Pax-FAK interactions extend this foundation.

In this report, we will specifically study the interaction between the full length Pax and the truncated targeting sequence of FAK. We will demonstrate that the binding energy between Pax and FAT can be quantified in vitro and is in close agreement with other published in vitro measurements. We further seek to study whether, and how, the interaction between our protein pair of interest is affected by a step change in strain applied to its substrate.

2. Materials and Methods

2.1. Cell preparation

Bovine aortic endothelial cells (BAECs) were cultured in Dulbecco's Modified Eagle Medium (DMEM) (Gibco, Invitrogen, Carlsbad, CA) supplemented with 10% fetal bovine serum,1% penicillin/streptomycin, and 1% L-glutamine. Cells were seeded at an initial density of 160,000 cells/well in fibronectin-coated 35mm glass-bottom (#1.5) dishes (MatTek Corporation, Ashland, MA). Transfection was carried out at ~80% confluence with either or both GFP-Paxillin (GPax), FAT-mCherry (FATmCh) plasmids, using the FuGene6 transfection reagent from Roche Diagnostics (Indianapolis, IN) and manufacturer's transfection protocols. Note that plasmid notation indicates position of fluorophore within the fusion protein, whereby GFP is at the N- terminus of Paxillin and mCherry is at the C-terminus of FAT. Lifetime imaging was carried out 24 h after transfection. For the study of chemical interruption to stretch induced mechano-response, we added 2 μM cytochalasin D (Sigma-Aldrich, MO) for 30 mins prior to imaging or with 100 μM Genistein (EMD Biosciences, CA) for 60 mins prior to imaging. Just before imaging, cells were washed with

PBS and DMEM supplemented with 10% fetal bovine serum, 1% penicillin/streptomycin, and 1% L-glutamine but with no phenol red was replaced in the wells.

2.2 Plasmids

GPax plasmids were obtained as a gift from K. Yamada of the NIH, Bethesda, MD. Mouse FAT from the dsRed-FAT plasmid (N. Mochizuki, National Cardiovascular Center Research Institute, Japan) was amplified by PCR with primer pairs (5-CTAAGCAACCTGTCCAGCATCAGC3-) and (5-CGGATCCGGGTGTGGCCGTGTCTGCCCTAGC3-). The resulting PCR fragment was ligated into pcDNA4/HisMax© TOPO® vector (Invitrogen, Carlsbad, CA). mCherry from the pRSET-B mCherry plasmid (R. Tsien, UCSD) was digested with EcoRI and BamHI and ligated into the pcDNA4-FAT vector at the 3′ end of FAT. The FAT-mCherry plasmid was amplified using the Qiagen MaxiPrep kit (Qiagen, Valencia, CA).

2.3. Biaxial stretch experiment

A schematic of our stretch device is found in Fig.1. Once assembled, cells are in an enclosed, sterile compartment, suitable for long-term monitoring. Another significant advantage is that the distance between the membrane, where cells are plated, and the glass coverslip is held constant while stretch is applied. This is important in order to ensure focus on the cell adhesion plane is not lost during stretch application, especially since cell position changes in the x-y plane with applied stretch. The device produces an equibiaxial strain profile [39].

A 2″ × 2″ silicon sheet (Specialty Manufacturing, Inc., MI) was affixed to the membrane holder with 1/16″ O-ring (McMaster-Carr, NJ). Wells were cut from a 0.5″ thick piece of PDMS and adhered onto the silicon sheet (Fig. 1 inset). Surface contact is sufficient to provide a good seal between the membrane and PDMS. This assembly was incubated with 5 μg/ml fibronectin applied to the membrane for 2 h before cell seeding and transfection. To assemble the device for imaging, high vacuum grease (Dow Corning, was applied to the outer edge of a #1 glass coverslip (VWR, PA) and the coverslip was carefully lowered into the base and firmly attached to the bottom, resulting in a complete seal around the coverslip. 2 ml and 0.3 ml DMEM with no phenol red was added to the base and cells respectively. Castrol grease (Structure Probe, Inc, PA) was applied to the piston tip to ensure good lubrication and facilitate slip between the piston tip and the membrane during strain application. The cell culture assembly was affixed to the piston by screws (McMaster-Carr, NJ), being very careful to use a spacer to prevent the piston from applying strain to the membrane at this time. The PDMS piece was removed and the whole assembly was inverted and lowered into the base, having first removed the spacer. Care was taken to ensure that no air bubbles were trapped between the membrane and the glass coverslip. The piston was affixed to the base with set screws. The entire stretch device was calibrated by measuring ink marks on the membrane as stretch is applied. The application of a 10% step strain requires about 40s due to the need for manual adjustment.

2.4 Microscopy imaging instrumentation

The custom-built two-photon microscope, as previously published [40], is based on a modified inverted microscope, Axiovert 110 by Zeiss (Göttingen, Germany), with a femtosecond laser source from the Mira family of modelocked Ti:Sapphire oscillators by Coherent (Santa Clara, CA). The laser excites a subfemtoliter volume at the focal point of a 40× Fluar objective (1.3NA, Zeiss).

For lifetime imaging [41-43], the laser is tuned to 890nm with 40mW power to excite GFP paxillin before the objective, resulting in low power at the sample so as to minimize photobleaching and cell damage. In order to minimize contributions from scattered laser light and autofluorescence, the cell's fluorescence signal is selected with a short-pass Schott BG-39 filter and short-pass 700nm filter from Chroma (Rockingham, VT). The signal is sent to the top port of the microscope where it is filtered for green wavelengths with HQ500LP from Chroma (Rockingham, VT). A photomultiplier tube (PMT), R7400P from Hamamatsu (Bridgewater, NJ), detects emitted photons and this signal is sent to a time-correlated single photon counting card (TCSPC card), SPC-730 from Becker-Hickl (Berlin, Germany). With 890 nm excitation, the m-Cherry FAT signal in doubly transfected cells is virtually undetectable in comparison with the GFP paxillin signal. For doubly transfected cells, fitting the lifetime dynamics of the donor to a double exponential decay will allow recovery of the lifetimes of the free and bound donor molecules as well as their relative intensity fraction.

For intensity imaging and FCS, a PMT with higher photon detection efficiency, H7421 from Hamamatsu (Bridgewater, NJ) is used in the bottom port of the microscope and is combined with single photon counting electronics. The laser is tuned either to 890nm (40mW before the objective) or 780nm (20mW before the objective). Power is low to minimize photobleaching throughout imaging. Green wavelengths from the cell are selected with BG-39 and SP700 filters (Chroma, Rockingham, VT) while red wavelengths are selected with two SP700 and a BP590-35 filters (Chroma, Rockingham, VT).

2.5 Imaging procedures

FCS calibration is needed to related intensity measurements to number concentrations. Intracellular FCS was carried out on cells transfected singly with either GPax or FATmCh. Intensity images of the same cells were also taken. FCS calibration factors, effective volume (V_{eff}) and shape factor $(r_0/z_0)^2$, were obtained using an aqueous solution containing 10 nM Alexa Fluor 488 (Molecular Probes, Eugene, OR) imaged in 8-chamber Lab- Tek® II, #1.5 coverglass slides (Thermo Fisher Scientific, Waltham, MA).

Double-transfected cells with fluorescent intensities in the middle range as observed using a 432 nm diode laser (Laserglow Technologies, Ontario, Canada) were selected for complete sets of intensity-FLIM imaging. We attempted to select for cells that were not over-expressing fusion proteins at too high a level but that were bright enough such that lifetime decay curves would have sufficient photon counts and acceptable signal-to-noise ratio (SNR). We found that the selected cells typically have fusion protein concentrations in the tens of nM to μM range when the associated images were analyzed using FCS calibrated

intensity measurements. These doubly transfected cells are typically slightly less bright than singly transfected cells (within a factor of 2).

For stretching experiments, cells are first plated in the stretch device. Initially, a complete set of intensity-FLIM images was taken, 10% strain was applied, and another complete set of intensity-FLIM images was taken for the same cells. The imaging protocol is identical for chemical disruption experiments, with imaging commencing after the above-mentioned incubation times. The experimental timeline is presented in Fig. 2. An equilibration time after application of step strain of 5 min was chosen as FAK phosphorylation was shown to peak at 5 min after application of stretch [44].

2.6 Data analysis

FLIM/FRET data were analyzed using the global analysis algorithm that was described extensively in our previous publication [43]. Briefly, from GPax transfected cells, the non-FRETting lifetime, τ_D, of GFP is obtained using a single-exponential fit to lifetime decays. This value is fixed when analyzing double-transfected cells. Resulting double-exponential fits retrieve the FRETting lifetime, τ_F, from which efficiency of energy transfer, E, can be calculated as shown in equation (5). A lower photon count limit of 500 photons/pixel was used when selecting pixels for which to fit decay curves.

FCS autocorrelation curves were analyzed with MATLAB (The MathWorks, Natick, MA) using the lsqnonlin nonlinear least-squares curve fitting function. A mean filter with a 5 × 5 kernel was used. While having the effect of reducing the effect of noise on resulting calculations, this step also results in loss of resolution (blurring) especially at image edges.

3. Theory/Calculation

3.1. Overview

It is well demonstrated that FRET and FCS allow in vitro detection of protein binding and the quantification of bound complex conformation [45-47]. Detecting the presence and absence of protein binding is clearly an important first step. While it is possible that mechanical forces will affect protein binding in a binary fashion; it is more likely that mechanotransduction mechanisms will up- or down-regulate protein binding affinity in the signaling pathways. From the thermodynamics standpoint, protein binding affinity is quantified by the steady-state dissociation constant and the associated Gibb's free energy. Although the measurement of protein binding affinity is routine in purified protein solutions, these measurements remain a challenge within living cells. A number of prior studies using FRET have partly overcome this difficulty. Hoppe and co-workers have developed an intensity based imaging methods allowing the quantification of ratio of bound and free proteins in equilibrium [48]. Subsequently, other investigators have extended this work by taking into account of the law of mass action to quantify the dissociation constant of interacting proteins [49, 50]. One limitation of these studies is that while relative dissociation constants can be determined, the absolute magnitudes cannot be measured. A landmark study overcoming these problems used two-photon cross correlation spectroscopy and enabled protein dissociation constants to be measured in living cells at selected locations [17]. We describe in the following section the theoretical basis for extending this approach

to quantitatively map the thermodynamic parameters of protein binding in living cells based on FRET microscopy and intensity imaging calibrated by FCS.

As an overview, BAECs were transiently transfected with fusion proteins: GPax and FATmCh (Fig. 3). Assuming steady state and the expression of fusion species is high relative to native protein, the interaction between GPax and FATmCh can be described by the following stoichiometric equation:

$$GPax + FATmCh \leftrightarrow FATmCh - GPax \quad (1)$$

One-to-one binding is assumed and is consistent with in vitro data [51] and published results based on FCS [38]. Given the reaction stoichiometry, the dissociation constant of FATmCh-GPax binding can be determined via the law of mass action:

$$K_d = \frac{C^{FATmCh} C^{GPax}}{C^{FATmCh-GPax}} \quad (2)$$

Lifetime-resolved imaging of donor fluorescence from GPax allows the quantification of FRET process. In a dynamic equilibrium as described by equation (1), GFP fluorescence will be generated by free, unbound GPax as well as GPax found to FATmCh. The unbound GPax will have fluorescence lifetime of GFP in the absence of FRET. The bound GPax will have shortened lifetime due to the presence of FRET to mCherry. Quantitative FRET imaging further allows a measure of the relative concentrations of bound, $C^{FATmCh–GPax}$, and free, C^{GPax}, paxillin [43]. Intensity measurements coupled with FCS calibration at the green and red emission channels quantify the number concentrations of the green ($C^{FATmCh–GPax}$ and C^{GPax}) and red ($C^{FATmCh–GPax}$ and C^{FATmCh}) fluorescent species, respectively. These three measurements provide three equations relating the three unknown product and reactant concentrations. Simultaneously solving these equations on a per pixel basis then determines the distribution of the dissociation constant, and the associated Gibb's free energy (ΔG), throughout the cell.

3.2. Quantification of cytoplasmic protein concentration based on FCS calibrated intensity measurements

The concentrations of green and red diffusing species in the cytosol are proportional to the fluorescence intensities measured. Intensity maps in the green and red channels can then provide a molecular concentration map of the green and red fluorescent proteins.

These proportionality constants can be determined based on FCS calibration. FCS measurement results in a fluctuating temporal sequence of fluorescence intensities, $F(t)$, due to thermally driven diffusion of fluorophores in-and-out of the two-photon excitation volume. This temporal sequence is analyzed through the normalized temporal autocorrelation function, $G(\tau)$, that is given by

$$G(\tau)=\frac{\langle \delta F(t) * \delta F(t+\tau)\rangle}{\langle F(t)\rangle^2} \quad (3)$$

where $\delta F(t) = F(t) - \langle F(t)\rangle$ and $\langle F(t)\rangle=\frac{1}{T}\int_0^T F(t)\,dt$. The autocorrelation curve is fit with the equation

$$G(\tau)=\frac{G(0)}{(1+\frac{t}{t_D})\sqrt{1+(\frac{r_0}{z_0})^2 * \frac{t}{t_D}}} \quad (4)$$

which describes freely diffusing fluorescence molecules in an approximate 3D Gaussian excitation volume. $G(0)=\frac{1}{\langle N\rangle}=\frac{1}{V_{eff}\,\langle C\rangle}$, N is the number of particles, V_{eff} is the effective focal volume, $(\frac{r_0}{z_0})^2$ is the shape factor a measure of the aspect ratio of the focal volume (r_0 = radius, z_0 = height), and τ_D is the diffusion timescale of the molecules, related to the molecule diffusion constant, D, by $\tau_D=\frac{r_0^2}{4D}$. Therefore, intracellular measurement of the autocorrelation function will allow us to determine *G(0)* and hence the concentration, <*C*>, of the molecules in the excitation volume if all the calibration factors are known. The calibration factors, effective volume (V_{eff}) and shape factor $(r_0/z_0)^2$, can be obtained independently using an aqueous solution containing a known concentration of dye.

3.3. Calculation for protein binding thermodynamic constants

For intracellular interaction of GPax and FATmCh, the binding reaction has stoichiometry as described by equation (1). The law of mass action (equation 2) can be generalized with spatial dependence and the dissociation constant, K_d, can be calculated:

$$K_d(x,y)=\frac{C_{cell}^{GPax}(x,y) * C_{cell}^{FATmCh}(x,y)}{C_{cell}^{GPax-FATmCh}(x,y)} \quad (5)$$

Here *C* denotes concentration.

In order to calculate K_d for this reaction, it is necessary to measure concentrations, or ratios of concentrations, of free and bound fluorescent species. As was shown in Pelet et. al [42], equation (6) presents the per-pixel fluorescence intensity decay measured by FLIM in a FRET system.

$$I(t)=\int_0^t G(t-T)\{\alpha_D e^{-T/\tau_D}+\alpha_F e^{-T/\tau_F}\}dT \quad (6)$$

I(t) is a convolution of the sum of the exponentials with the instrument response *G(t)*. Pre-exponential factors α_D and α_F reflect fractional contributions to the total fluorescence from

the free donor (no FRET) and bound donor (with FRET) species respectively, each of which undergoes decay at rates τ_D and τ_F.

$$\frac{\alpha_F}{\alpha_D+\alpha_F}=\frac{C_{cell}^{GPax-FATmCh}}{C_{cell}^{GPax}+C_{cell}^{GPax-FATmCh}}=FR \quad (7)$$

a_D and a_F are the fractional fluorescent intensities of the free and bound donor species, the ratio of which is the same as the ratio of the concentrations of bound and free GPax within the pixel. We denote this term as the FRET ratio (FR).

In addition, the FRET efficiency, *E*, that characterizes bound molecule conformation, can be obtained from the recovered lifetimes:

$$E=1-\frac{\tau_F}{\tau_D} \quad (8)$$

This FRET ratio from equation (7) can be related to the ratio of C_{cell}^{GPax} / $C_{cell}^{GPax\text{-}FATmCh}$.

$$1+\frac{C_{cell}^{GPax}}{C_{cell}^{GPax-FATmCh}}=\frac{1}{FR} \quad (9)$$

$$\frac{C_{cell}^{GPax}}{C_{cell}^{GPax-FATmCh}}=\frac{1}{FR}-1 \quad (10)$$

The concentration ratio as obtained in equation (10) can be substituted into equation (5), resulting in the following expression:

$$K_d(x,y)=C_{cell}^{FATmCh}(x,y)*(\frac{1}{FR(x,y)}-1) \quad (11)$$

The dissociation constant can be measured if we can measure the concentration of free FATmCh. However, it is non-trivial to measure the concentration of free FATmCh in a doubly-transfected cell since any contribution measurement in either the green or red channel will contain contributions from both the free protein and the bound complex. However, as will be shown below, by measuring the concentration of both green and red emitting species, the concentration of the free FATmCh can be determined algebraically.

In principal, the concentration of the red and green emitting species can be determined intracellularly by FCS. However, since FCS measurement is slow, it is impractical to map these concentration distributions throughout the cell. Instead, intensity maps will be obtained throughout the cell and FCS calibrations will be performed to measure the brightness of the green and red emitting species allowing the conversion of intensity values to number concentrations. The concentration distribution of either the red or green species can then be obtained by calibrating the intensity images with the known brightness.

$$C^i_{cell}(x,y)=\frac{I^i(x,y)_{cell}}{<I^i_{calib}>}*<C^i_{calib}>=I^i(x,y)_{cell}*\frac{1}{<B^i_{calib}>} \quad (12)$$

Here, *i* can be either red (*R*) or green (*G*) fusion proteins, making no distinction between free and bound species, $I^i(x, y)$ is the intensity of the cell at location *(x,y)* in units of photons per unit time, $<I^i_{calib}>$ is the average intensity of singly transfected cells in the calibration experiment, $<C^i_{calib}>$ is the average concentration of fusion protein in singly transfected cells in the calibration experiment. The molecular brightness of the fluorescent protein in the cell as measured by our instrument can be defined as:

$$<B^i_{calib}>=\frac{<I^i{}_{calib}>}{<C^i{}_{calib}>}$$

There are two additional complications due to the presence of FRET and spectral bleedthrough. When converting from intensity to concentration, green channel intensities arise from GFP excitation. For free GPax, the directly measured signal can be calibrated from (9). For bound GPax, there is energy transfer to FATmCh and the fluorescence contribution from bound GPax is reduced by the FRET efficiency, E. Intensities in the red channel contain contributions from both free and bound FATmCh, as well as some bleed-through, β from the green channel, that is subtracted.

The green channel intensity excited at 890 nm is given by,

$$I^G_{ch}(x,y)=I^{GPax}_{cell}(x,y)+(1-E)I^{GPax-FATmCh}_{cell}(x,y)=I^G_{cell}(x,y) \quad (13)$$

The green species concentration is given by

$$C^{GPax}_{cell}(x,y)+(1-E)C^{GPax-FATmCh}_{cell}(x,y)=C^G_{cell}(x,y) \quad (14)$$

The red channel intensity excited at 780 nm is given by

$$I^R_{ch}(x,y)=I^{FATmCh}_{cell}(x,y)+I^{GPax-FATmCh}_{cell}(x,y)+\beta k I^G_{cell}(x,y) \quad (15)$$

The last term is the bleedthrough of GFP excited at 780 nm to the red channel. β is the factor quantifying the the spectral bleedthrough from the excited GFP into the red channel. In order to related this quantity to the green channel intensity detected at 890 nm as defined in equation (13), we further need a calibration factor *k* that related the ratio of the brightnesses of GFP excited at 780 nm relative to being excited at 890 nm. The brightness ratio *k* is a constant calibration factor that was determined from singly transfected GFP cells.

The red species intensity is given by

$$I^R_{cell}(x,y)=I^{FATmCh}_{cell}(x,y)+I^{GPax-FATmCh}_{cell}(x,y)=I^R_{ch}(x,y)-\beta k I^G_{cell}(x,y) \quad (16)$$

Finally, the red species concentration is given by

$$C^{FATmCh}_{cell}(x,y)+C^{GPax-FATmCh}_{cell}(x,y)=C^R_{cell}(x,y) \quad (17)$$

From equations (10) and (14),

$$C^{GPax-FATmCh}_{cell}(x,y)=\frac{C^G_{cell}(x,y)}{(\frac{1}{FR(x,y)}-E)} \quad (18)$$

Combining this with equation (17), we obtain

$$C^{FATmCh}_{cell}(x,y)=C^R_{cell}(x,y)-\frac{C^G_{cell}(x,y)}{(\frac{1}{FR(x,y)}-E)} \quad (19)$$

A final substitution in equation (11) gives us K_d.

$$K_d(x,y)=(\frac{1}{FR(x,y)}-1)*(C^R_{cell}(x,y)-\frac{C^G_{cell}(x,y)}{(\frac{1}{FR(x,y)}-E)} \quad (20)$$

Using this methodology, which combines FLIM and intensity-concentration scaling, K_d can therefore be calculated for entire cells. A conversion to the Gibbs free energy of binding naturally follows from $\Delta G = RT$ 1n K_d. R is the universal gas constant, 8.314 $JK^{-1}mol^{-1}$, and T is the temperature of the system, 300 K.

4. Results

4.1 FCS intensity-concentration calibration

FCS was carried out on 5 different GPax cells, totaling 26 repeated measurements, while for FATmCh cells, FCS was carried out on three different cells, totaling 38 repeated measurements. Representative autocorrelation curves and the resultant fit from each cell set are presented in Fig. 4. The GPax autocorrelation curves were fit with a single component fit, while the FATmCh curves were fit with a single component plus a constant term fit. As can be seen from Fig 4, G(0) values are similar, thus signifying similar intracellular protein concentrations in both groups of cells. mCherry is a dimmer fluorophore compared to GFP [52, 53], and care must be taken to remove autofluorescence signals. In any case, mCherry autocorrelation curves are noiser. These points are also reflected in the intensity-concentration values calculated as following: $\langle I^G_{calib}\rangle = 1.1\times10^5 \pm 1.6\times10^4$ photons/second, $\langle C^G_{calib}\rangle = 24.22 \pm 6.00$ nM, $\langle I^R_{calib}\rangle = 8.8\times10^3 \pm 2.5\times10^3$ photons/second, $\langle C^R_{calib}\rangle = 30.03 \pm 17.45$ nM. The brightnesses are: $\langle B^G_{calib}\rangle = 4.5\times10^3$ photons/second/nM and $\langle B^R_{calib}\rangle = 2.9\times10^2 \pm 1.8\times10^2$ photons/second/nM. The brightness of mCherry is significantly lower than that of GFP due to both fluorophore photochemistry as well as the

lower sensitivity of our imaging system in the redder spectral range. The uncertainties in these calibration values are due to measurement noise including uncertainties in measuring G(0) due to shot noise and due to position variations in cells in the presence of some non-diffusing proteins. Examining the effect of these uncertainties in the measurement of Δ*G*, the uncertainty in the resultant Δ*G* is approximately 5% of the mean value. The typical fusion protein concentrations of PaxG and FATmCh are found to range from tens of nM to μM range.

4.2 Single cell calculation of ΔG

A histogram of average lifetimes comparing a single-transfected GPax cell with a double-transfected cell demonstrates a shift to lower average lifetimes in double-transfected cells (Fig. 5). This is consistent with the occurrence of FRET and fusion protein binding.

A representative dataset from a single cell measurement is shown in Fig. 6. Fig. 6 (a) and (b) show the intensity images of red and green species within the cell. After brightness calibration as discussed in Section 3.2, the mean concentrations of both green and red species are in the 500 nM range. Fig. 6(c) shows the cell pseudo-colored by FR distribution, the ratio of free to bound GPax, based on global analysis on FLIM data. Global fitting of FLIM data further allow the extraction of two fitted lifetimes of τ_D = 2.60 ns and τ_F = 1.94 ns. The resultant τ_F / τ_D ratio of 0.75 gives a FRET efficiency, E, of 0.2 and an interfluorophore distance of 56Å. Fig. 6(d) shows that the distribution of dissociation constant measured in the cytosol is approximately 209 ± 50 nM. Fig. 6(e) shows the resultant cell map once ΔG has been calculated. Averaging over the whole cell, ΔG = -38 ± 5 kJ/mol.

4.3 Effect of FRET ratio scaling and mean filtering

FR values can be skewed at low intensity pixels during global analysis [43]. One solution is to set an intensity threshold at a high level such that low intensity pixels are ignored but that often left us with few workable pixels per cells. We have developed an FR scaling method that can correct for this skew, allowing us to work with many more pixels at lower intensity, as discussed in our previous publication [43]. In addition to FR scaling, we also found that mean filtering is very effective in removing noise in our thermodynamic parameter calculations. Here, we evaluate and demonstrate the effects of FR scaling and mean filtering. For mean filtering, we found that for increasing kernel size, ΔG and its variance decrease to a plateau value. A kernel size of 5 × 5 strikes a balance between increasing loss of spatial resolution and decreasing noise. This is shown for a representative cell in Fig. 7(a), which tracks the effect of increasing kernel size on the distribution of ΔG. Number of neighbors in the plot refers to the number of surrounding rows of pixels that are averaged over, whereby neighbor number of 2 corresponds to a 5 × 5 kernel size. FR scaling slightly decreases the mean value of ΔG. The effect of FR scaling and mean filtering on ΔG distribution is further shown Fig. 7 (b). It can be seen that FR scaling clearly increases the number of pixels captured in the final ΔG image while mean filtering significantly narrows the distribution of ΔG.

4.4. Measuring ΔG across multiple cells

It is also important to evaluate our consistency in extracting thermodynamic parameters from cells with the same preparation protocol over time. A plot of ΔG values calculated for ten cells measured on three separate days is given in Fig. 8. It can be seen that there is variation in the ΔG measured from cell to cell, up to 10%. These ΔG values correspond to an average K_d value of 366.9 ± 33.7 nM. This study shows that the dissociation constant can be reliably measured by our method despite minor variances in culture conditions.

4.5. The effect of the presence of native proteins

The levels of fusion protein expression are critical. On one hand, fusion protein expression levels should not be too high to minimize their physiological effects on cells. One the other hand, the fusion proteins should be expressed at sufficiently high levels relative to the native proteins. This is important because we have assumed a law of mass action that involves only three interacting species (equation 2). We have performed Western blot analysis and show that this assumption is true with fusion proteins expressing at a level at least ten times that of endogenous Pax and FAK (Fig. 9). Qualitatively, the expression levels of native proteins are approximately over an order of magnitude lower than that of the fusion proteins. In addition to the native Pax and FAK, both Pax and FAK may have other protein binding partners. Interactions with these other proteins may also partly compromise the assumptions made in the law of mass action. Here, we make the assumption that the fusion protein expression levels are also high relative to these other native proteins. Given our need to express fusion proteins well above native level, it is reasonable to question whether over-expression affects native biological processes. We may note that the overall morphology and actin distribution are not significantly differ between transfected cells and wide-type cells. However, more subtle changes in cellular physiology cannot be ruled out. We may note that this shortcoming is common in many cellular studies involving fluorescent proteins with the exception of some correlation spectroscopy measurements where expression levels can be kept fairly low.

Within these limits of fusion protein expression levels, there is also concern that expression level differences in different cells may affect our measurement accuracy. While one may reduce expression level difference by synchronizing the cells under study, however, we note that protein expression levels can remain quite stochastic in nature even with synchronized cells. Further, protein concentration at different locations within even a signal cell can be large and may be greater than cell-to-cell variances. Therefore, we stress that our methodology must be robust in recovering “intrinsic” parameters of protein interactions independent of fusion protein expression level. These intrinsic parameters, that characterize molecular level properties of protein interaction, include FRET efficiency E (characterizing bound protein conformation), the dissociation constant, k_d, and the Gibbs free energy, G, should be independent of protein expression ratio. Further, there are other “extrinsic” parameters, such as FRET ratio, FR, that should dependent on local fusion protein expression levels governed by the law of mass action. Fig. 10 demonstrates the robustness of our approach in recovering the correct intrinsic parameters in the presence of intracellular fusion protein concentration variation. In this figure, the concentration, [FATmCh], is plotted against concentration ratio, [FATmCh-PaxG]/[PaxG], for different pixel within a

single cell. According to the law of mass action, the instantaneous slope is the dissociation constant, k_d of the protein and should be constant independent of reactant concentration. The linearity of the plot demonstrates that this constancy of k_d for [FATmCh] concentration ranging from 50 nM to over 200 nM ([PaxG] distribution also has a similar range). There may also be concerns that low fluorescence signal intensities, associated with regions of low protein distribution, will affect FRET measurement accuracy; this issue has been discussed extensively in our previous publications [43] where we show that with the imaging condition and analysis protocol used, accurate FRET measurements can be performed.

Finally, the presence of fusion proteins bound to endogenous binding partners may result in a distortion of the FCS autocorrelation curves and the resultant fits. In terms of the effect on G(0) value, since the concentration of endogenous species is low, we do not expect endogenous protein binding to greatly affect molecular mass and hence diffusion rate. Approximating the diffusing fluorescent species as a homogenous sphere, its hydrodynamic radius scales by the cube root of the molecular weight [54, 55]. Thus, a change in the diffusion rate by a factor of two will require an increase of eight times in the mass of the fusion protein due to binding of non-fluorescent native species. That is quite unlikely due to the similar sizes of proteins, even in the case of FATmCh due to the presence of the fairly large m-cherry. Therefore bound and unbound fusion proteins will exhibit diffusion times on the same scale, averaging to one G(0) value in our measurements. In fact, our diffusion curves fit well to the diffusion of a single species.

4.6. Comparison between FA and cytosol

We check to see as well if there are any significant differences between ΔG values calculated at FAs compared to ΔG values calculated in the cytosol. One might expect there to be some difference in the distribution of these ΔG values as FAs are mechanically and biochemically different environments compared to the cytosol. Traction forces exerted by cells onto the glass substrate presumably are transferred through the actin cytoskeleton intracellularly and are transmitted to the substrate via focal adhesions, since these are the sites of cell attachment to the substrate. The cytosolic region does not ‘feel’ this force. A specific subset of proteins localize to FAs compared to those present in the cytosol, thus potentially resulting in different binding characteristics between GPax and FATmCh.

FA and cytosolic regions within cells were identified and separately grouped based on intensity segmentation. While FAs are always brighter than the immediate surrounding cytosol, FA intensities are not the same throughout the whole cell. Some bright cytosolic regions might be as bright as some FA regions in other parts of the cell. Each cell is thus first segmented into regions with similar FA and cytosolic intensities, before further segmentation into separate FA and cytosolic regions. An example is shown in Fig. 11, which shows the original intensity image (Fig. 11 (a)) and the same cell segmented into FA (red), cytosol (blue), and unselected regions (black) (Fig. 11 (b)). After segmentation, we can compare FRET and thermodynamic measurements between FA and cytosol regions. While there might be slight differences in ΔG between FA and cystol for some cells, there is no clear trend for a larger population (Fig 12).

4.7. Effect of step strain on ΔG

A 10% step strain was applied and ΔG values were calculated and compared for the same cell before and after strain. Comparisons between cell intensity before and after applied stretch show a 35.9% decrease in GPax intensity (Fig. 13(a)), and a much smaller decrease of 5.5% in FATmCh intensity (Fig. 13(b)). Directly from FLIM global analysis fits, it can be seen that FR shifts to higher values upon stretch, on average 0.072 ± 0.008, or 18.6% (5 cells) indicating tighter binding. Shifts are significant for all pairs (student t-test). A representative histogram of FR distribution for cells under static and stretch conditions demonstrates this (Fig. 13 (c)). A lower histogram height upon stretch, corresponding to fewer total pixels, is also an indication of the loss in GPax intensity, since the same intensity threshold cutoff (500 counts per pixel) was used in both cases when selecting pixels for which to carry out FLIM analysis. Besides this, there was also a difference in fitted FRET lifetime, τ_F, the lifetime being lower by 4.8% upon stretch. A lower τ_f corresponds to a slight conformational change that brings the fluorophores closer by 2 Å. This tighter conformation is consistent with the tighter binding observation indicated by FR shift.

The effect of 10% step strain on ΔG values for 5 different cells is shown in Fig. 14(a). Overall, there is a shift to lower ΔG values upon application of stretch, whereby all shifts are significant (student t- test) except for one pair. Overall, a reduction of 5 ± 1% is observed. A lower ΔG value corresponds to a smaller K_d, which indicates a tighter binding interaction. Grouping all ΔG values together before and after stretch before carrying out comparisons also results in similar conclusions.

In order to verify that the change is real, complete intensity-FLIM measurements were carried out on cells cultured in the stretch device, with a time interval of 15 min between complete sets, but without application of stretch. 15 min corresponds to the average time it usually takes between static and stretch imaging of the same cells. ΔG values were then compared. This is to remove the effect of time as a potential factor in the change seen in ΔG values. Results of this are shown in Fig. 14(b). The one pair with a significant change shows a change in the opposite direction to the change observed upon stretch. Therefore, overall there is no significant change in ΔG values. FLIM global analysis fits also show no significant change in either τ_F or FR. This confirms our observation that the application of stretch results in an enhancement of GPax – FATmCh binding.

4.8. Effect of chemical disruption on stretch-induced ΔG

A very interesting observation that can be made related to the changes in ΔG values we measure is that it reflects global changes occurring throughout the cell, since we average values over the whole cell. Therefore, the effect of force that is directed into the cell through the FAs is translated into signals that are able to propagate throughout the whole cell. This most likely points to some kind of soluble factor(s) effect. There are many factors that could give rise to the change seen in ΔG values, including direct mechanical effect [56], a phosphorylation enzyme effect [57] [58], Ca^{2+} signaling [59], and oxidative stress [60]. It might well be impossible to specifically tease out the actual factor(s) that effects changes seen in ΔG values. However, it is possible to try and negate the changes seen, by blocking

specific processes within the cells and examining how the response changes (or not). We biochemically alter the cell by adding either cytochalasin D or genistein to the system.

Cytochalasin D acts by capping the barbed end actin of actin filaments while allowing depolymerization at the pointed end to still occur. This results in dismantling of the intracellular actin network as shown in Fig. 15(a). Genistein is an ATP-competitive tyrosine kinase inhibitor, the addition of which therefore blocks any potential tyrosine phosphorylation signaling within the signal transduction cascade. Addition of genistein to the system does not result in any observable morphological changes (Fig. 15(b)), or changes in actin filament organization.

The effect of adding these two biochemical reagents (cytochalasin D: 4 cells, genistein: 6 cells) to the system is quantified in Fig. 16. For all the sub-figures, the percentages represent changes occurred between the first (after 8 min) and the second (after 23 min) FLIM imaging sections (see Fig. 2). The odd bars (from left) corresponds to cells that have been subjected to bi-axial strain with procedure as described in Fig. 2. The even bars correspond cells that the strain application step is replaced by a period passively waiting. The left two bars are cells in standard medium without drug treatment. The middle two bars are cells subjected to cytochalasin D treatment. The right two bars are cells subjected to gerinstein treatment. Firstly, the results of FLIM global analysis fits are plotted in Fig. 16(a) whereby the percentage difference in τ_F obtained for fits on static and stretched cells are compared. As previously explained, stretch leads to shortening of τ_F, corresponding to a decrease in interfluorophore distance. Merely adding a time interval does not significantly change the lifetime, nor does addition of cytochalasin. This means that with these two treatments, interfluorophore distance remains constant. Addition of genistein brings back the decrease in interfluorophore distance. Next, the overall percentage difference in ΔG values calculated under static and stretch conditions are plotted in Fig. 16(b). Lastly, a pixel-by-pixel percentage difference in ΔG values was calculated and plotted in Fig. 16(c). As can be seen, all plots display a similar overall trend. A positive stretch response corresponds to a decrease in interfluorophore distance, i.e. the proteins are holding on to each other slightly tighter. Merely adding a time interval between images removes the effect of stretch on calculated ΔG values. Addition of cytochalasin D results in a slight lowering of the stretch response while the addition of genistein does not alter the stretch response.

From our data, blocking of Tyr phosphorylation does not block the stretch response. This means that it is not the Tyr phosphorylation pathways that lead to stretch-induced signaling, as applied to our system of GPax – FATmCh binding. It might seem that cytochalasin D slightly reduces the stretch response. If this is indeed true, changes in GPax – FATmCh binding is caused in part by a direct physical effect of the applied mechanical force. A look at the lifetime data also leads us to postulate that physical changes in protein conformation (at least partially) gives rise to the changes seen in ΔG.

5. Discussions

5.1. Implications on the roles of Pax and FAK on mechanotransduction

In this work, we have demonstrated a method to quantify intracellular protein binding based on FRET imaging and intensity measurement calibrated with FCS. This approach allows us to determine whether protein binding exists, the fraction of protein bound, the bound protein conformation, and the binding thermodynamics. It is important to be certain that the binding thermodynamic parameters are reasonable. We have measured a mean dissociation constant between paxillin and FAT to be 367±33 nM. In vitro measurement of K_d values for the FAT-LD domain interaction have been published. Gao et. al measured a K_d of ≈ 10 μM for the interaction between a synthetic LD peptide and the FAT domain by ITC [61]. Thomas et. al. measured a K_d of ≈ 4 μM for a similar interaction, though using the SPR technique [51]. These values are an order of magnitude higher than our new measurements in vitro. Very interestingly, when both LD2 and LD4 are present in the protein construct, Thomas and co-workers found that the interaction between this construct and FAT is much tighter, resulting in a measured K_d of 300 – 600 nM [51] in close agreement with our measurement. Thomas et. al. attribute this increase in binding affinity to the presence of both LD domains, suggesting an allosteric effect on protein binding. While the presence of one LD domain can result in binding between FAT and this domain, the presence of both LD domains strengthens binding roughly tenfold, indicating positive cooperativity. Clearly, our experiment involves the whole FAT sequence where both LD2 and LD4 domains are present and we expect similar allosteric effect. It is interesting to note that allosteric effects observed in vitro appear to be also important intracellularly. It might be time to rethink our understanding of intracellular inter-protein interaction. Current methods used to predict or depict protein binding, for example molecular dynamics simulation [62, 63] or protein docking software [64, 65], are capable only of modeling small proteins or protein segments solvated usually in water. Conclusions obtained from these computational methods should thus always be carefully evaluated against the realities of an inherently complex intracellular environment where proteins are packed together and where binding interactions with multiple protein partners complicate the simplified one-to-one binding interaction usually depicted in computational models.

It is also interesting to note that contrary to expectations, differences that do exist between FA and cytosol do not appear to affect GPax / FATmCh binding. From in vitro binding experiments, it is known that the LD2-LD4 fragment and FAT readily associate in solution. It could be that in the cellular system, GPax and FATmCh associate in the cytosol and the complex is recruited to FAs by GPax's other binding partners, the binding of which does not affect the GPax-FATmCh interaction. If this were the case, then even at the FA, free FATmCh can freely associate or exchange to bind GPax at the same rate that binding occurs in the cytosol. It is also possible that since we are using only the targeting sequence FAT instead of the full length protein, FAK, FAT only binds to Pax and is not a portion of the normal force transduction pathway that a normal FAK would be a part of. In this case, it may be logical to expect that there is no force across the Pax-FAT linkage and the dissociation constant differs little from that of Pax and FAT in cytosol. It is important to note that our results are also at variance with recent FCS based studies by Digman et al. and

Choi et al. where they found that Pax and FAK interactions occur only at the FAs but not in the cytosol [36, 38]. This variance may be due to the different choice of cell type being studied (fibroblasts vs endothelial cells). However, it may be more likely that this discrepancy is due to the fact that we are studying only the FAT fragment while full length FAK was used in the other studies. Consistent with the conjecture that regulation by the rest of the FAK sequence can play a role, Choi and coworkers found that this protein binding interaction is strongly dependent on protein phosphorylation state where they found no FAK cytosolic interaction with nonphosphorylatable Pax mutant (Y31F-Y118F) but found robust interaction with phosphomimetic Pax mutant (Y31E-Y118E) [38].

In this work, we show that application of external mechanical force in the form of equibiaxial strain results in a shift in ΔG to lower values, corresponding to smaller K_d and thus tighter protein binding, between our proteins, GPax and FATmCh, compared to static conditions. This change directly correlates with a change in τ_F. In other words, the change in ΔG values correlate with change in interfluorophore distance, which we interpret to directly reflect changes in average inter-protein distance between GPax and FATmCh. One may note that we have attributed the change in FRET efficiency entirely to a change in inter-fluorophore distance. This assumption is of course an over simplification as FRET efficiency can also be modified due to factors such as change in fluorophore orientation and rotational dynamics. A more precise characterization of strain induced conformation change in the bound complex will have to await future work utilizing polarization resolved FRET imaging. In any case, FRET efficiency is a sensitive method to detect the presence of molecular conformation change due to mechanotransduction.

Comparing the stretch experiments to controls with measurements taken over the same time interval demonstrates that time alone cannot explain the observed changes. In order to explore other potential sources of change, biochemical disruption was affected by adding either cytochalasin D or genistein, to either disrupt the actin cytoskeleton network or to block Tyr phosphorylation. While genistein has no significant effect on blocking the stretch response, observations related to cytochalasin D are not as conclusive. The response is reduced slightly, though statistical significance cannot be established. In any case, we can conclude that phosphorylation is not a key factor in strain response o f Pax-FAT strain response.

It is also important to note that the effects of strain are seen globally throughout the cell independent of whether measurement is made at the FA or in the cytosol. One potential explanation is that within the 5 min allowed for equilibration, fusion proteins at FAs are continuously modified and cycle out into the cytosol at a rate governed by the fusion protein turnover rate at FAs. Published fluorescence recovery data of GFP-Pax in FAs [66] shows that the k_{off} for GFP-Pax is 0.015 s^{-1} when the recovery curve is fit with an exponential as demonstrated by Lele et. al [56]. Given a best case estimate of FA area being 10% of total basal membrane area at the adhesion plane (based on Fig. 10), and FA height being 10% of cell height, FA volume is roughly 1% of cell volume. FA intensity is on average 1.5 times cytosol intensity at the adhesion plane, as seen also in Fig. 10. Thus in total, the number of fusion proteins in all FAs is 0.015 times the number of fusion proteins in the cytosol. In order to replace all cytosolic fusion proteins with fusion proteins modified at the FA, 66.7

turnover events are required. Within the 5 minutes allowed for equilibration, the total number of turnover events is $5 \times 60 \times 0.015 = 4.5$. Even allowing for the 22 minutes it takes to complete an imaging set (Fig. 3), this number increases only to 20. Therefore this is an unlikely explanation for our results.

We attribute the effect of strain on Pax-FAT binding to soluble factor(s) with cytosol concentration(s) that is(are) strain dependent. One possible factor is talin. Though we have shown that endogenous Pax and FAK expression levels are much lower compared to fusion protein expression levels, this may not be true for other native proteins such as talin. It is possible that under stretch conditions, competitive binding of talin for FATmCh may displace GPax, thus affecting FATmCh-GPax binding.

Even with chemical disruption, the magnitude of change in ΔG values calculated correlates with the change in fit τ_F. This really is a major strength in our measurement technique. With our technique, the origin of change in measured thermodynamic constants can hereby be directly linked to changes in inter-protein distances, thus relating the mechanotransduction phenomena to molecular conformational change.

5.2. Additional discussions on assumptions and limitations of this work

While we have shown that FRET is a powerful method to quantify intracellular protein interactions, this approach is based on many assumptions and thus has certain limitations. The main assumption made in this work that allows us to formulate the equations for our system is that the system is under thermodynamic equilibrium. While the cell might remain relatively static, internal processes that occur might affect local environments, and thus binding events, for example changes in the rate of fusion protein translation. However, the assumption of thermodynamic equilibrium within cells is reasonable considering the much longer timescale for translation, and most other cellular processes, compared to our measurement timescale.

Results from FCS intensity-concentration calibration are based on the implicit assumption that the fluorescent species observed diffusing in and out of the focal volume are of the same species, all of which are free molecules available for binding. This would be false if other proteins bind to the fusion proteins in such a way to prevent subsequent GPax-FATmCh interaction. If the levels of all endogenous protein expression are much lower than fusion protein expression, this factor can be ignored. While this can be shown to be true for endogenous Pax and FAK compared to GPax and FATmCh as shown in Fig. 9 above, and extrapolating to other endogenous proteins lead us to the same conclusion, this point cannot be definitively proven for comparisons between protein species. If the expression levels of some endogenous fusion protein binding partners, such as talin are indeed comparable to fusion protein expression levels, their binding will affect our result as discussed previously.

Our imaging procedure takes at best 16 mins. The bottleneck in the imaging sequence lies in the time it takes to acquire a sufficiently good FLIM dataset. This time is governed by the need to acquire data for a sufficiently long time in order to build up decay curves with enough photon counts and good SNR. Excitation power is kept low so as to not cause damage to the cell. Within this imaging time frame, the cell undergoes many processes, the

most obvious of which is morphological change and motion. Due to this, our calculations should be considered an average measure over both space and time. This time could be reduced by further improvements in FLIM techniques. One example is to carry out video rate FLIM [67, 68]. One could also explore the possibility of multifocal multiphoton [69] or temporal focusing [70] FLIM which would acquire images at multiple points in the sample simultaneously, thereby reducing the image acquisition time and removing motion artifacts.

Our measured intracellular K_d values are reasonable compared to in vitro measurements, though a direct comparison is not necessarily accurate given the differences in both actual proteins used, and in microenvironment inhabited. Expected differences between FA and cytosolic measurements were not observed, leading to the conclusion that the binding interaction proceeds similarly at the FA and in the cytosol, probably due to the GPax-FATmCh complex being perched to the side of the direct traction force transmission pathway. It would be highly advantageous if a separate method could be used to verify our results. The use of two fluorophores in our system suggests that it would be possible to apply the TPCCS method as published by Kim et. al. [17] in order to achieve this verification. This would essentially involve carrying out FCS measurements on double-transfected cells and quantifying the autocorrelation and cross-correlation amplitudes in order to back out binding stoichiometry. The capability of carrying out spectrally resolved fluorescence correlation spectroscopy based on global analysis (SRFCS-G) [71] readily lends itself to this measurement technique.

6. Conclusions

By developing a new fluorescent spectroscopic assay, the mechanosensitivity of Pax-FAT binding reaction have been characterized both structurally and thermodynamically. We have demonstrated that imposing an external strain results in larger fraction of Pax bound to FAT and forming more compact molecular complex with tighter binding characteristics. This mechanosensitivity can be abolished by partly relaxing intracellular strain by disrupting the actin cytoskeleton. Spatially resolved mapping suggests that this effect is mediated by diffusible molecular factors instead of direct force-induced protein deformation. While the identification of these molecular factors provides interesting future research directions, we have further excluded protein phorphorylation enzymes as responsible for the observed mechano-sensitivity.

Although the development of this new spectroscopic assay is motivated by studying Pax-FAT interaction, this technique is generally applicable to study intracellular protein interactions in a broad class of cellular biological problems. This technique is built upon prior FRET studies [49]. By including FCS calibrated intensity information, this technique allows the determination of the absolute magnitude of dissociation constants and other thermodynamic variables. The use of lifetime based method further allows more precise determination of relative concentrations of bound and free protein fractions in cells. This method is complementary to two-photon cross-correlation spectroscopy (TPCCS) [17] that can also quantify intracellular binding affinities quantitatively but only at selected locations inside cells. This FRET based assay affords greater experimental efficiency and enables protein binding affinity to be imaged with 3D resolution in living cells. Importantly, this

technique further provides molecular structural information of the bound complex allowing the changes in inter-protein distances to be correlated with protein binding changes in affinity and energies. While significant progress is made in the quantitative study of protein interaction in cells, studying the Pax-FAK system highlights some of the future challenges. First of all, Pax and FAK both have over ten different protein binding partners and many of these binding processes may exhibit allosteric character. While many binding assays are geared towards studying binary interactions, they are ill matched to understand these complex interactions in vivo. Second, many quantitative affinity assays, especially image based assays, are relatively slow taking seconds to minutes while many cellular processes exhibit significantly faster dynamics. Improving the speeds of these binding assays is important. Finally, signal to noise consideration often requires over-expression of the proteins of interest in many assays resulting in biological systems that may be far from their native states. The development of assays with molecular sensitive that can work with fluorescent proteins in their native concentration remains a priority.

Acknowledgments

PTCSO acknowledges supports from: NIH 9P41EB015871-26A1, R01-EX017656, 5 R01 NS051320, 4R44EB012415-02, NSF CBET-0939511, the National Research Foundation Singapore through the Singapore MIT Alliance for Research and Technology's BioSym research programme, the Singapore-MIT Alliance 2, the MIT SkolTech initiative, the MIT-Dana Fabre Cancer Center Bridge Funding, The McGovern Institute Neurotechnology (MINT) program, and the Hamamatsu Corporation. The authors would also like to thank Prof. Keith Berland of Emory University for his invaluable suggestion in combining intensity imaging with FCS calibration to quantify the concentration of green and red diffusing species in the cells.

References

1. Gosling JP. Clin Chem. 1990; 36:1408–1427. [PubMed: 2201458]
2. Morgan CL, Newman DJ, Price CP. Clin Chem. 1996; 42:193–209. [PubMed: 8595711]
3. Leavitt S, Freire E. Curr Opin Struct Biol. 2001; 11:560–566. [PubMed: 11785756]
4. Velazquez Campoy A, Freire E. Biophys Chem. 2005; 115:115–124. [PubMed: 15752592]
5. Velazquez-Campoy A, Leavitt SA, Freire E. Methods Mol Biol. 2004; 261:35–54. [PubMed: 15064448]
6. Fielding L, Rutherford S, Fletcher D. Magn Reson Chem. 2005; 43:463–470. [PubMed: 15816062]
7. Fivash M, Towler EM, Fisher RJ. Curr Opin Biotechnol. 1998; 9:97–101. [PubMed: 9503595]
8. Homola J. Anal Bioanal Chem. 2003; 377:528–539. [PubMed: 12879189]
9. Rich RL, Myszka DG. Curr Opin Biotechnol. 2000; 11:54–61. [PubMed: 10679342]
10. Berland KM, So PT, Chen Y, Mantulin WW, Gratton E. Biophys J. 1996; 71:410–420. [PubMed: 8804624]
11. Berland KM, So PT, Gratton E. Biophys J. 1995; 68:694–701. [PubMed: 7696520]
12. Kettling U, Koltermann A, Schwille P, Eigen M. Proc Natl Acad Sci U S A. 1998; 95:1416–1420. [PubMed: 9465029]
13. Rarbach M, Kettling U, Koltermann A, Eigen M. Methods. 2001; 24:104–116. [PubMed: 11384186]
14. Ai HW, Shaner NC, Cheng Z, Tsien RY, Campbell RE. Biochemistry. 2007; 46:5904–5910. [PubMed: 17444659]
15. Chudakov DM, Lukyanov S, Lukyanov KA. Trends Biotechnol. 2005; 23:605–613. [PubMed: 16269193]
16. Shu X, Shaner NC, Yarbrough CA, Tsien RY, Remington SJ. Biochemistry. 2006; 45:9639–9647. [PubMed: 16893165]

17. Kim SA, Heinze KG, Bacia K, Waxham MN, Schwille P. Biophys J. 2005; 88:4319–4336. [PubMed: 15792970]
18. Foo YH, Naredi-Rainer N, Lamb DC, Ahmed S, Wohland T. Biophys J. 2012; 102:1174–1183. [PubMed: 22404940]
19. Shi X, Foo YH, Sudhaharan T, Chong SW, Korzh V, Ahmed S, Wohland T. Biophys J. 2009; 97:678–686. [PubMed: 19619483]
20. Sudhaharan T, Liu P, Foo YH, Bu W, Lim KB, Wohland T, Ahmed S. J Biol Chem. 2009; 284:13602–13609. [PubMed: 19293156]
21. Truong K, Ikura M. Curr Opin Struct Biol. 2001; 11:573–578. [PubMed: 11785758]
22. Wallrabe H, Periasamy A. Curr Opin Biotechnol. 2005; 16:19–27. [PubMed: 15722011]
23. Peter M, Ameer-Beg SM, Hughes MK, Keppler MD, Prag S, Marsh M, Vojnovic B, Ng T. Biophys J. 2005; 88:1224–1237. [PubMed: 15531633]
24. Parsons M, Monypenny J, Ameer-Beg SM, Millard TH, Machesky LM, Peter M, Keppler MD, Schiavo G, Watson R, Chernoff J, Zicha D, Vojnovic B, Ng T. Mol Cell Biol. 2005; 25:1680–1695. [PubMed: 15713627]
25. Huang H, Kamm RD, Lee RT. Am J Physiol Cell Physiol. 2004; 287:C1–11. [PubMed: 15189819]
26. Bao G, Kamm RD, Thomas W, Hwang W, Fletcher DA, Grodzinsky AJ, Zhu C, Mofrad MR. Mol Cell Biomech. 3:91–105. [PubMed: 20700472]
27. Geiger B, Avnur Z, Kreis TE, Schlessinger J. Cell Muscle Motil. 1984; 5:195–234. [PubMed: 6423268]
28. Geiger B, Bershadsky A. Cell. 2002; 110:139–142. [PubMed: 12150922]
29. Kaazempur Mofrad MR, Abdul-Rahim NA, Karcher H, Mack PJ, Yap B, Kamm RD. Acta Biomater. 2005; 1:281–293. [PubMed: 16701807]
30. Mofrad MR, Golji J, Abdul Rahim NA, Kamm RD. Mech Chem Biosyst. 2004; 1:253–265. [PubMed: 16783922]
31. Schaller MD. Oncogene. 2001; 20:6459–6472. [PubMed: 11607845]
32. Parsons JT. J Cell Sci. 2003; 116:1409–1416. [PubMed: 12640026]
33. Hayashi I, Vuori K, Liddington RC. Nat Struct Biol. 2002; 9:101–106. [PubMed: 11799401]
34. Digman MA, Brown CM, Horwitz AR, Mantulin WW, Gratton E. Biophys J. 2008; 94:2819–2831. [PubMed: 17993500]
35. Digman MA, Brown CM, Sengupta P, Wiseman PW, Horwitz AR, Gratton E. Biophys J. 2005; 89:1317–1327. [PubMed: 15908582]
36. Digman MA, Wiseman PW, Choi C, Horwitz AR, Gratton E. Proc Natl Acad Sci U S A. 2009; 106:2170–2175. [PubMed: 19168634]
37. Rossow MJ, Sasaki JM, Digman MA, Gratton E. Nat Protoc. 2010; 5:1761–1774. [PubMed: 21030952]
38. Choi CK, Zareno J, Digman MA, Gratton E, Horwitz AR. Biophysical Journal. 2011; 101:517–517.
39. Lee AA, Delhaas T, Waldman LK, MacKenna DA, Villarreal FJ, McCulloch AD. Am J Physiol. 1996; 271:C1400–1408. [PubMed: 8897847]
40. So PT, Dong CY, Masters BR, Berland KM. Annu Rev Biomed Eng. 2000; 2:399–429. [PubMed: 11701518]
41. Pelet S, Previte MJ, Kim D, Kim KH, Su TT, So PT. Microsc Res Tech. 2006; 69:861–874. [PubMed: 16924635]
42. Pelet S, Previte MJ, Laiho LH, So PT. Biophys J. 2004; 87:2807–2817. [PubMed: 15454472]
43. Rahim NA, Pelet S, Kamm RD, So PT. J Biomed Opt. 2012; 17:026013. [PubMed: 22463045]
44. Lehoux S, Esposito B, Merval R, Tedgui A. Circulation. 2005; 111:643–649. [PubMed: 15668343]
45. Jares-Erijman EA, Jovin TM. Nat Biotechnol. 2003; 21:1387–1395. [PubMed: 14595367]
46. Bacia K, Kim SA, Schwille P. Nat Methods. 2006; 3:83–89. [PubMed: 16432516]
47. Kim SA, Heinze KG, Schwille P. Nature Methods. 2007; 4:963–973. [PubMed: 17971781]
48. Hoppe A, Christensen K, Swanson JA. Biophys J. 2002; 83:3652–3664. [PubMed: 12496132]
49. Chen H, Puhl HL 3rd, Ikeda SR. J Biomed Opt. 2007; 12:054011. [PubMed: 17994899]

50. Kofoed EM, Guerbadot M, Schaufele F. J Biol Chem. 2010; 285:2428–2437. [PubMed: 19926790]
51. Thomas JW, Cooley MA, Broome JM, Salgia R, Griffin JD, Lombardo CR, Schaller MD. J Biol Chem. 1999; 274:36684–36692. [PubMed: 10593973]
52. Shaner NC, Campbell RE, Steinbach PA, Giepmans BN, Palmer AE, Tsien RY. Nat Biotechnol. 2004; 22:1567–1572. [PubMed: 15558047]
53. Shaner NC, Steinbach PA, Tsien RY. Nat Methods. 2005; 2:905–909. [PubMed: 16299475]
54. Haustein E, Schwille P. Methods. 2003; 29:153–166. [PubMed: 12606221]
55. Haustein E, Schwille P. Curr Opin Struct Biol. 2004; 14:531–540. [PubMed: 15465312]
56. Lele TP, Pendse J, Kumar S, Salanga M, Karavitis J, Ingber DE. J Cell Physiol. 2006; 207:187–194. [PubMed: 16288479]
57. Shikata Y, Rios A, Kawkitinarong K, DePaola N, Garcia JG, Birukov KG. Exp Cell Res. 2005; 304:40–49. [PubMed: 15707572]
58. Wang JG, Miyazu M, Matsushita E, Sokabe M, Naruse K. Biochem Biophys Res Commun. 2001; 288:356–361. [PubMed: 11606050]
59. Sokabe M, Naruse K, Sai S, Yamada T, Kawakami K, Inoue M, Murase K, Miyazu M. Heart and vessels. 1997; (Suppl 12):191–193. [PubMed: 9476580]
60. Howard AB, Alexander RW, Nerem RM, Griendling KK, Taylor WR. Am J Physiol. 1997; 272:C421–427. [PubMed: 9124284]
61. Gao G, Prutzman KC, King ML, Scheswohl DM, DeRose EF, London RE, Schaller MD, Campbell SL. J Biol Chem. 2004; 279:8441–8451. [PubMed: 14662767]
62. Gough CA, Gojobori T, Imanishi T. Proteins. 2007; 66:69–86. [PubMed: 17063491]
63. Lee SE, Kamm RD, Mofrad MR. J Biomech. 2007; 40:2096–2106. [PubMed: 17544431]
64. Bradford JR, Westhead DR. Bioinformatics. 2005; 21:1487–1494. [PubMed: 15613384]
65. Vajda S, Camacho CJ. Trends Biotechnol. 2004; 22:110–116. [PubMed: 15036860]
66. Cohen DM, Kutscher B, Chen H, Murphy DB, Craig SW. J Biol Chem. 2006; 281:16006–16015. [PubMed: 16608855]
67. Agronskaia AV, Tertoolen L, Gerritsen HC. J Biomed Opt. 2004; 9:1230–1237. [PubMed: 15568944]
68. Grant DM, Elson DS, Schimpf D, Dunsby C, Requejo-Isidro J, Auksorius I, Munro I, Neil MA, French PM, Nye E, Stamp G, Courtney P. Opt Lett. 2005; 30:3353–3355. [PubMed: 16389829]
69. Kumar S, Dunsby C, De Beule PA, Owen DM, Anand U, Lanigan PM, Benninger RK, Davis DM, Neil MA, Anand P, Benham C, Naylor A, French PM. OPT EXPRESS. 2007; 15:12548–12561. [PubMed: 19550524]
70. Choi H, Tzeranis DS, Cha JW, Clemenceau P, de Jong SJ, van Geest LK, Moon JH, Yannas IV, So PT. OPT EXPRESS. 2012; 20:26219–26235. [PubMed: 23187477]
71. Previte MJ, Pelet S, Kim KH, Buehler C, So PT. ANAL CHEM. 2008; 80:3277–3284. [PubMed: 18351754]

Highlights

- Demonstrated a new method to map protein interaction dissociation constant and Gibbs free energy distribution in living cells.
- Demonstrated that the fraction of bound proteins and their conformation can be measured in living cells.
- Demonstrated that paxillin-FAT interactions in vivo is allosteric.
- Demonstrated that paxillin-FAT interaction is mechanosensitive and this mechanosensitivity is mediated by soluble factors.
- Demonstrated that Paxillin-FAT mechanosensitivity is not based on protein tyrosine phosphorylation.

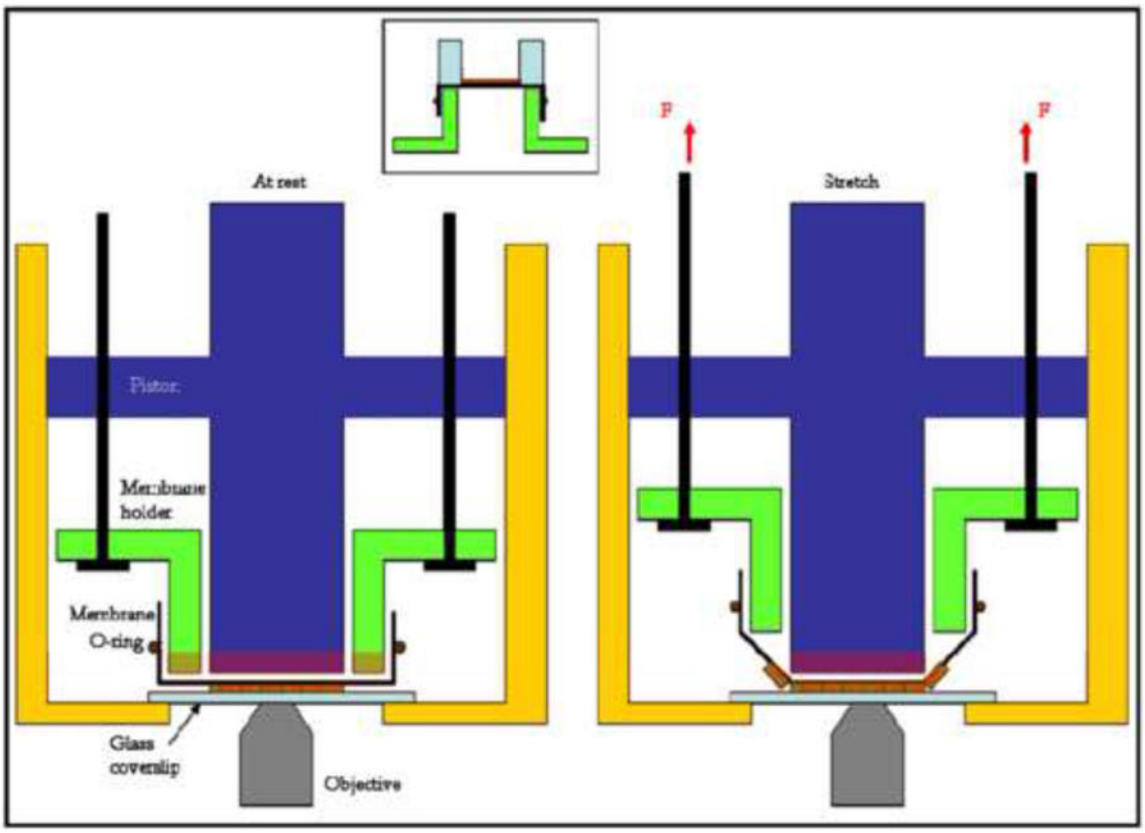

Fig. 1.

Schematic of the equibiaxial stretch device before and during applied stretch. Membrane holder orientation with cultured cells when in the incubator is shown in the inset.

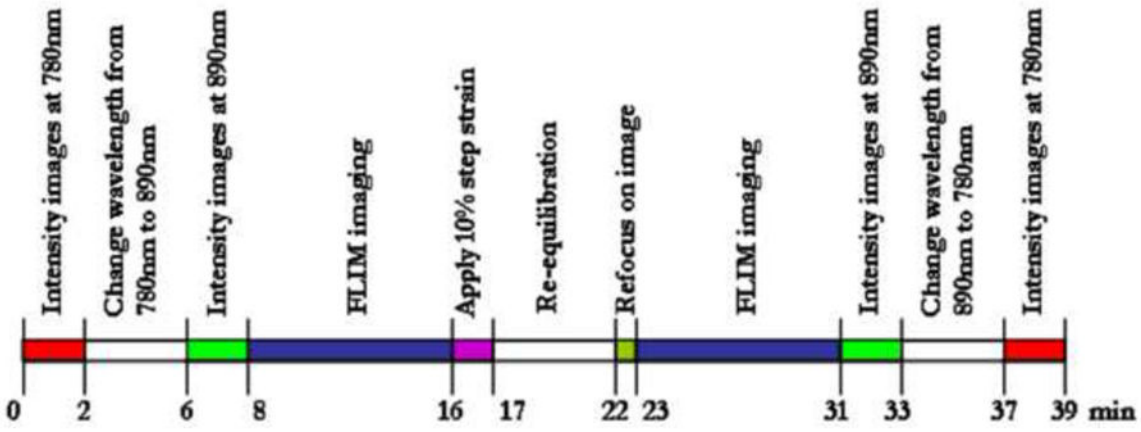

Fig. 2.
Timeline for the stretch experiment.

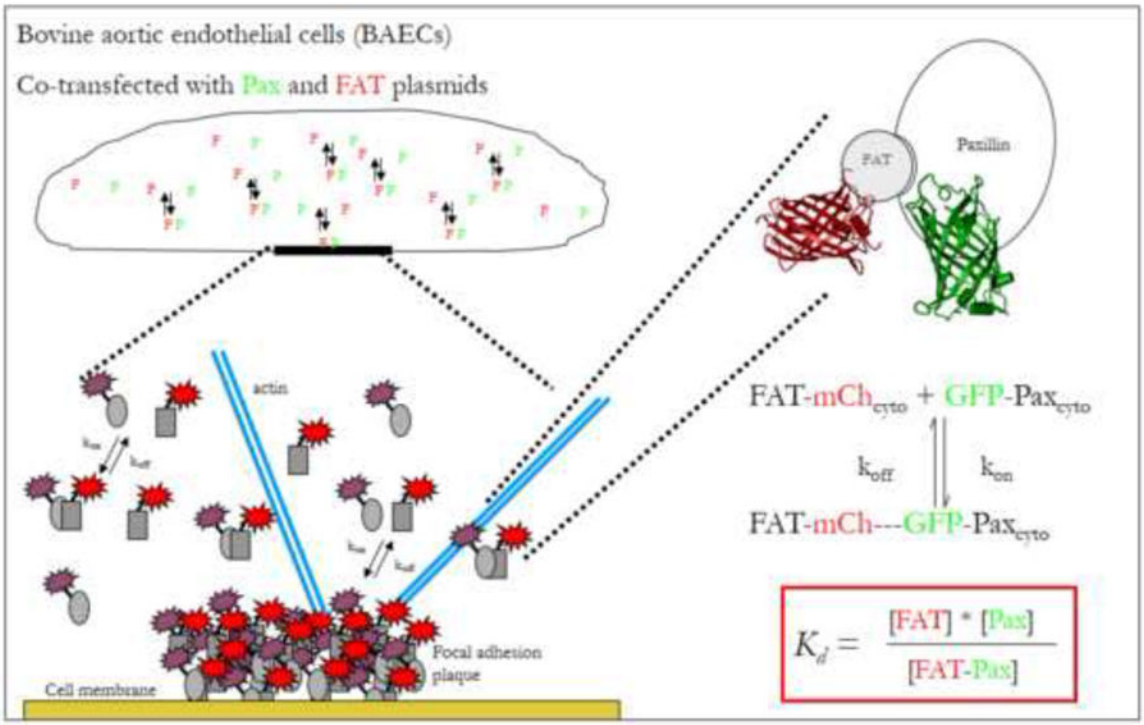

Fig. 3.
A simplified schematic representation of GPax and FATmCh equilibrium in BAECs.

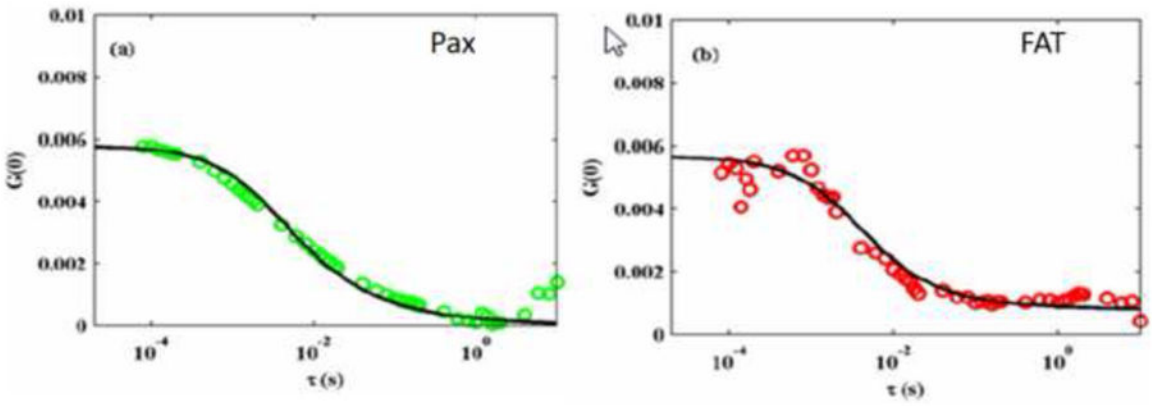

Fig. 4.
Representative FCS curves and resultant fit from (a) GPax or (b) FATmCh only cells.

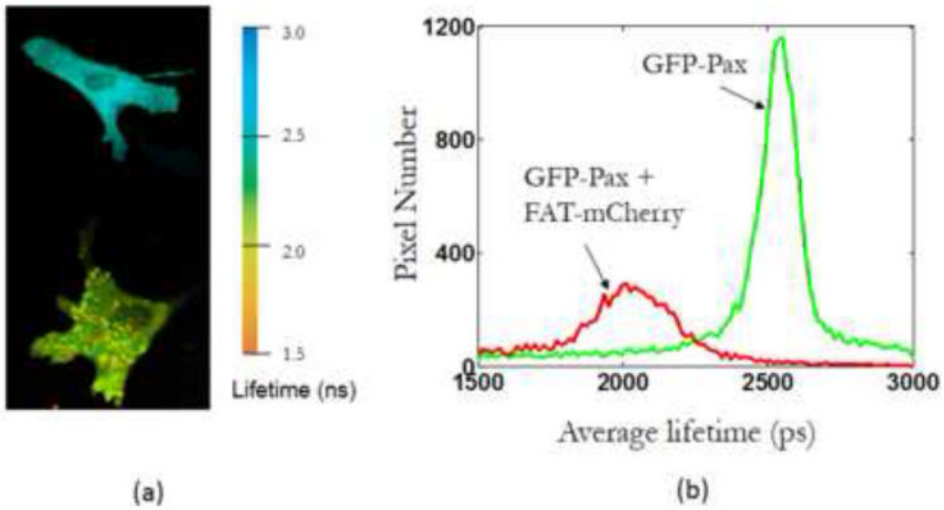

Fig. 5.

(a) Mean lifetime map of a cell transfected with only GPax (top) and a cell transfected with both GPax and FATmCh (bottom). (b) The lifetime distributions of the singly and doubly transfected cells.

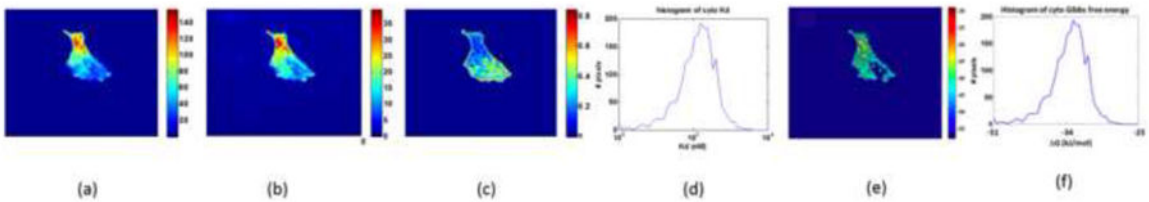

Fig. 6.

Representation measured and calculated image for a cell transfected with GPax an FATmCh. (a) Green channel intensity image, (b) Red channel intensity image, (c) FR distribution image, (d) histogram of Kd value distribution, (e) Gibbs free energy distribution image.

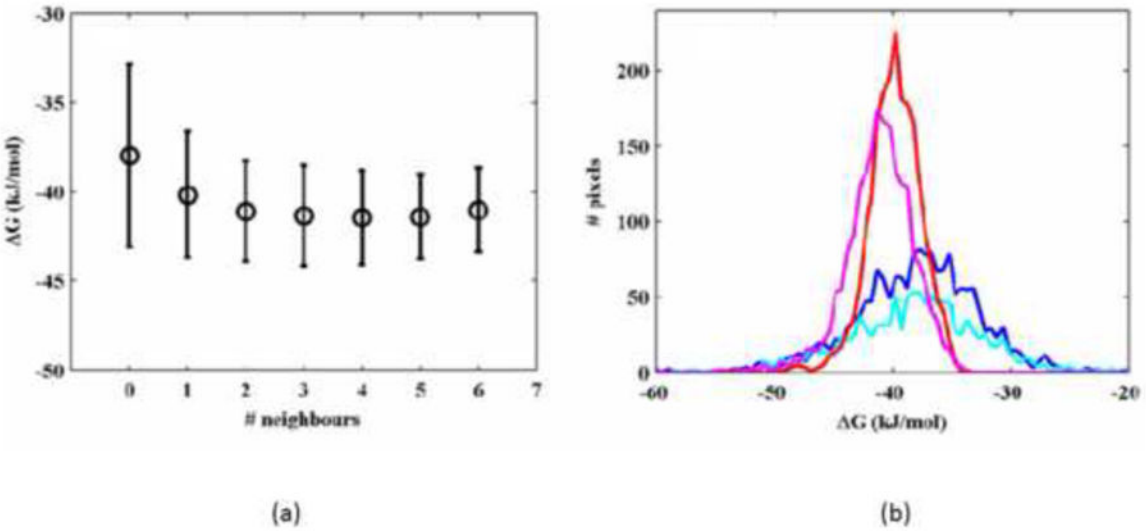

Fig. 7.

Effects of FR scaling and mean filtering on calculated ΔG values. (a) Plot of ΔG vs mean filtering kernel size. A neighbor number of two corresponds to a 5 × 5 kernel. Error bars indicate standard deviation. (b) Histogram of ΔG values with FR scaling and mean filtering. ΔG without FR scaling or mean filtering (blue), ΔG with just FR scaling (cyan), ΔG with just mean filtering (red), ΔG with both FR scaling and mean filtering (purple).

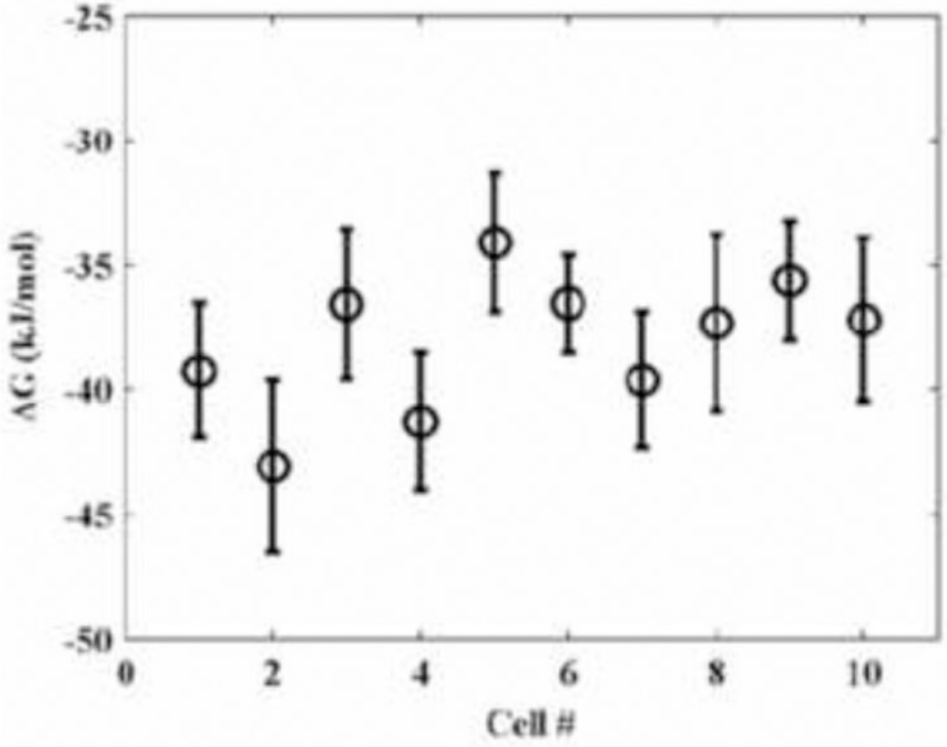

Fig. 8.
Consistency of ΔG measurements over ten cells.

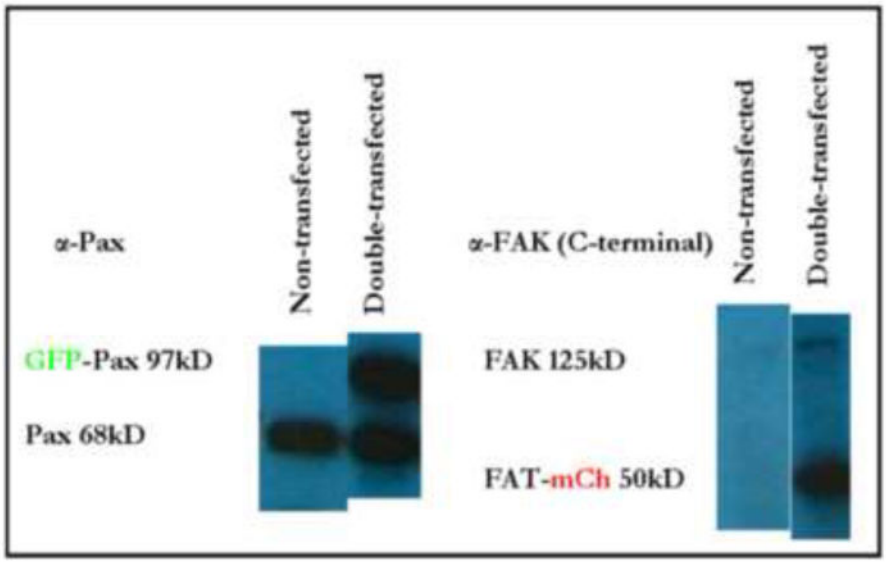

Fig. 9.
Western bolts comparing expression ratio of native and fusion proteins.

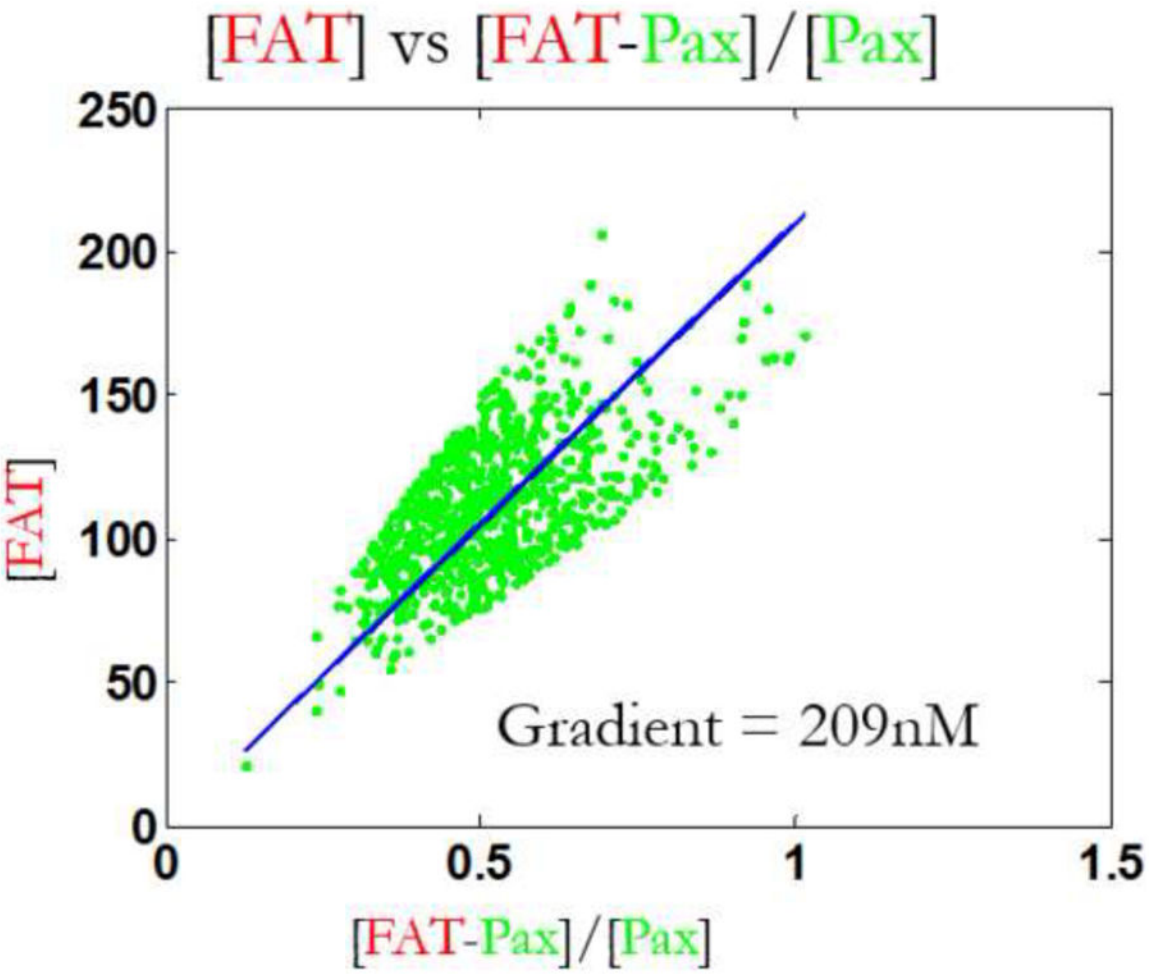

Fig. 10.

Concentration of FATmCh vs concentration ratio of FATmCh-PaxG and PaxG measured at different pixels of a single doubly transfected cell. A linear dependence is expected given one-to-one binding and the law of mass action. The slope corresponds to a dissociation constant of 209 nM.

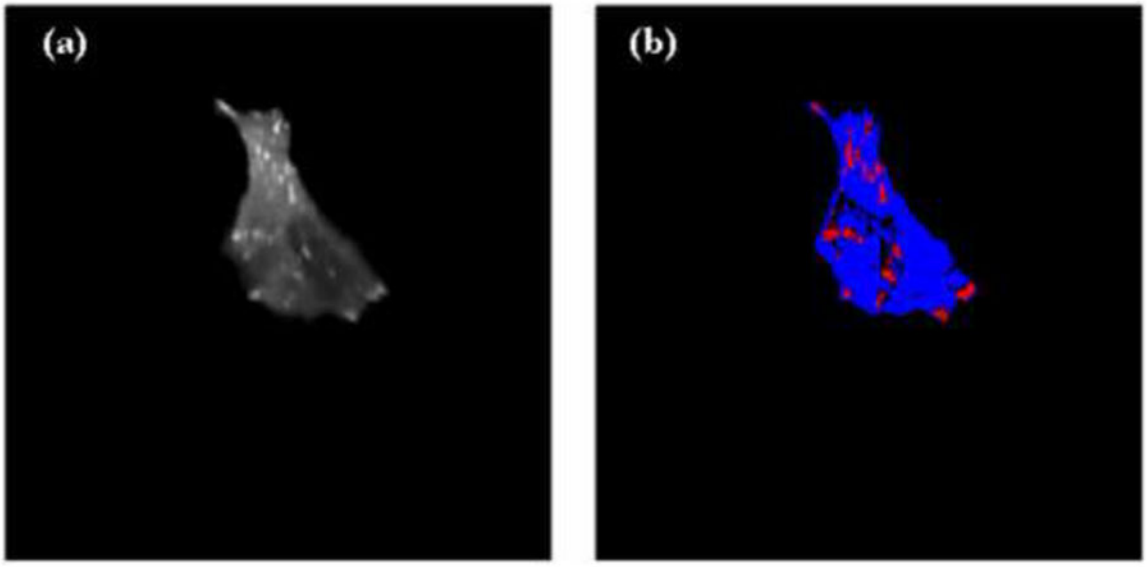

Fig. 11.

Intensity based segmentation for FA region and total basal membrane region. (a) Intensity gray scale image of a representative cell. (b) Segmented image of the same cell where red area corresponds to the FA region, blue area corresponds to the total basal membrane region, and black areas are pixels that have intensity below cutoff threshold.

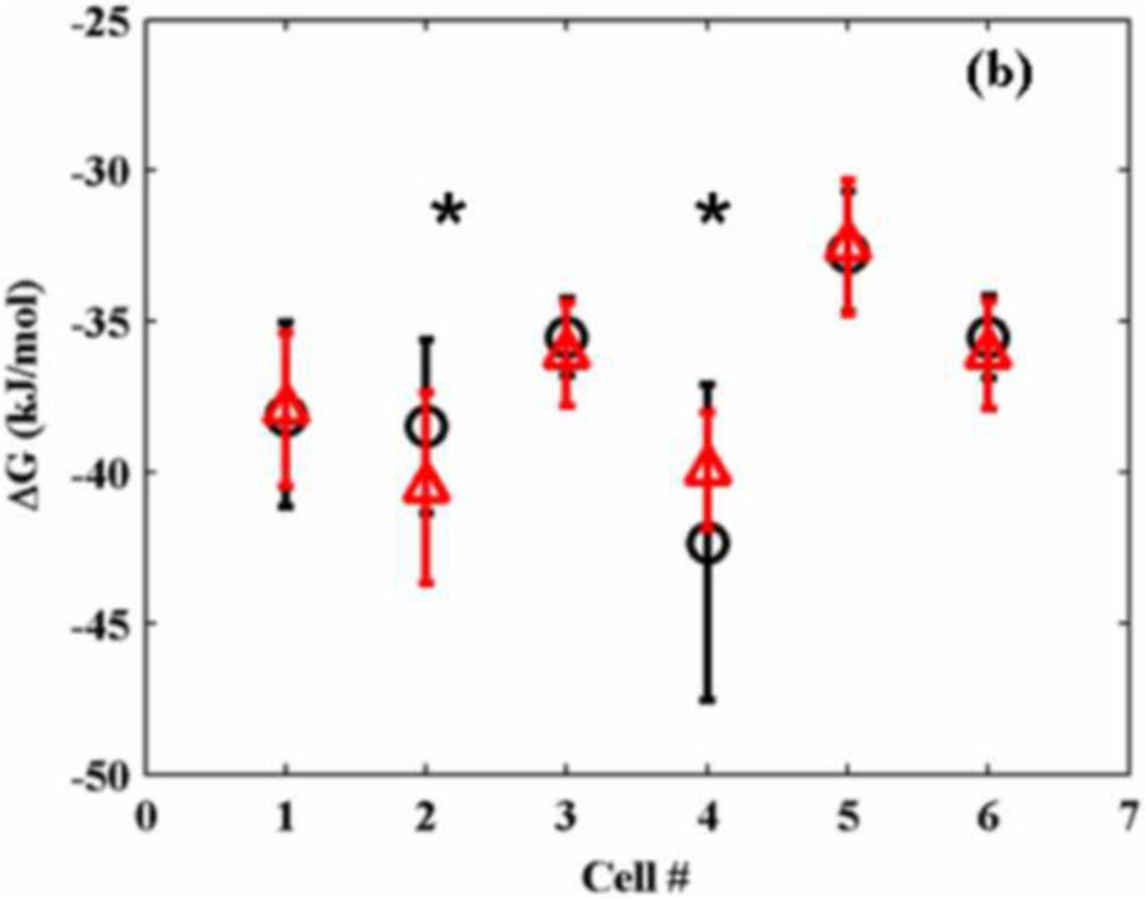

Fig. 12.

Comparison between ΔG values values measured at focal adhesions (circles) and values measured in the cytosol (triangles). Asterisks indicate statistical difference as measured by t-test with p-value < 0.05. Error bars denote standard deviation.

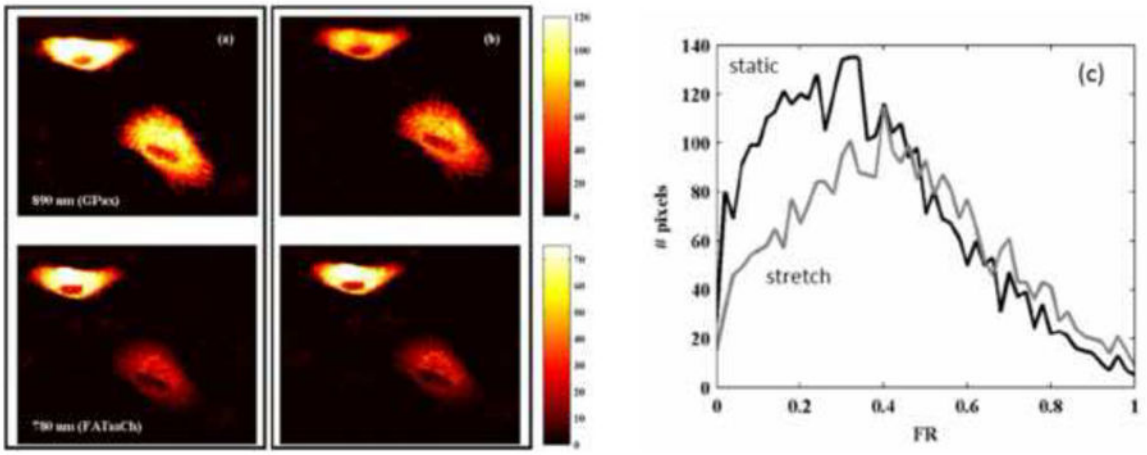

Fig. 13.

Representative stretch experiment. (a) GPax and FATmCh intensity distributions of representative cells before stretch, (b) GPax and FATmCh intensity distributions of representative cells after stretch, (c) FR histograms before and after stretch experiment.

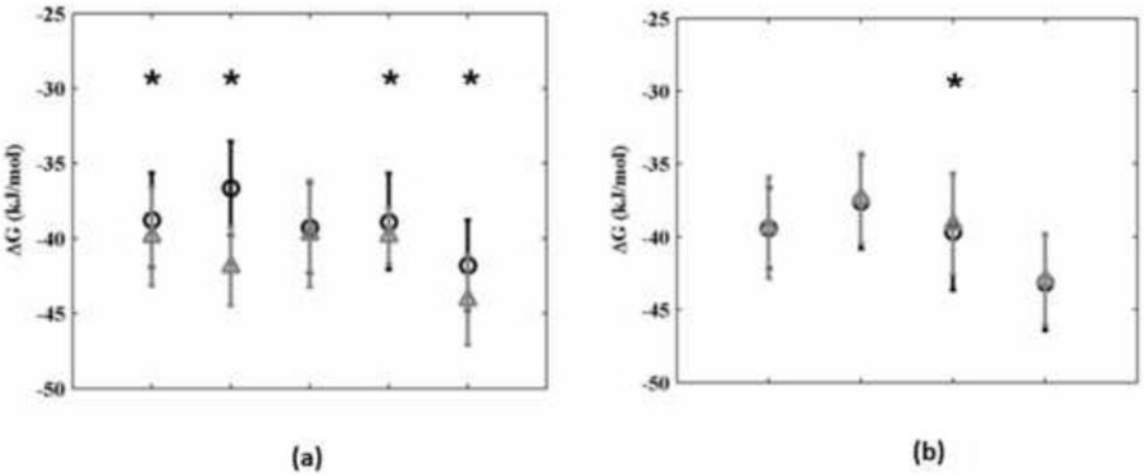

Fig. 14.

(a) Comparison of ΔG values calculated for 5 cells under static (circle) and 10% strain application (triangle). Significant difference is indicated, $P<0.05$. (b) Comparison of ΔG values calculated for static cells before (circle) and after (triangle) a 15 minute time interval. Significant difference is indicated, $P<0.05$.

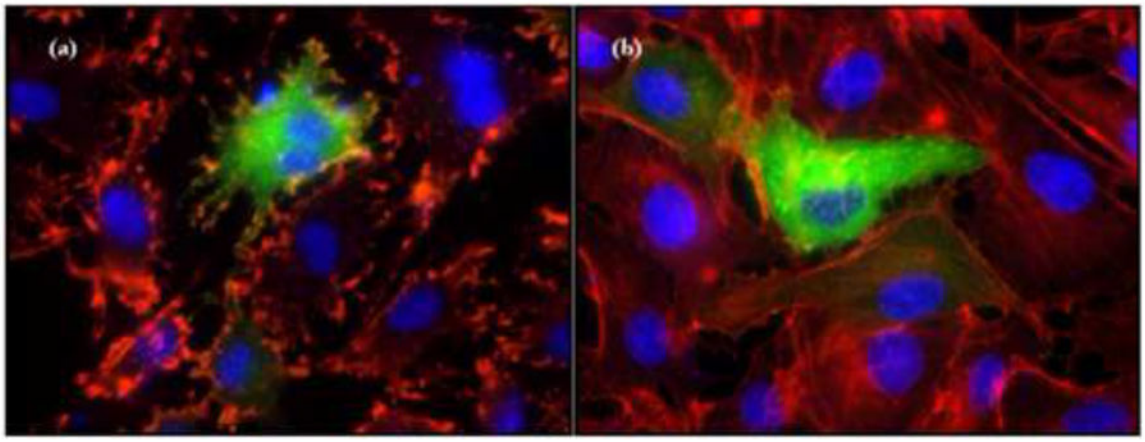

Fig. 15.

Images of cells plated on fibronectin-coated glass-bottom-dishes, transfected with GPax and fixed with 4% paraformaldehyde. Cells were stained with nuclear stain, DAPI (blue), and actin stain, rhodaminephalloidin (red). (a) Effect of cytochalasin D. (b) Effect of genistein.

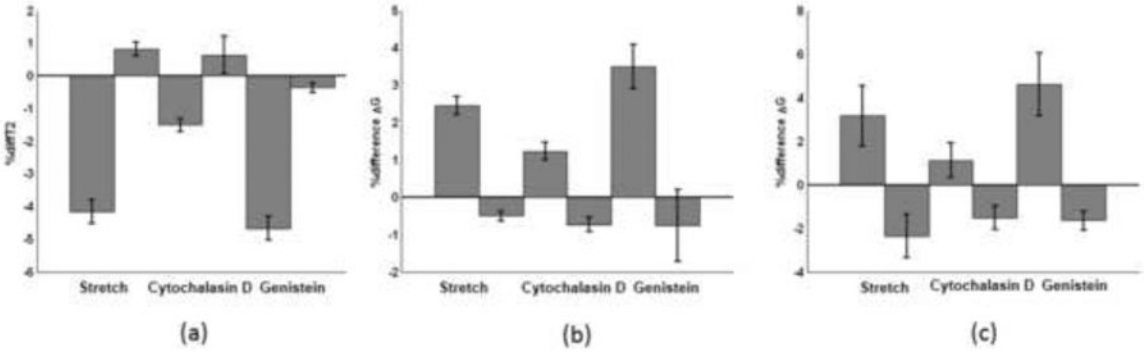

Fig. 16.

Stretch response under various biochemical inhibitor assays. For all the sub-figures, the percentages represent changes occurred between the first (after 8 min) and the second (after 23 min) FLIM imaging sections (see Fig. 2). The odd bars (from left) corresponds to cells that have been subjected to bi-axial strain with procedure as described in Fig. 2. The even bars correspond cells that the strain application step is replaced by a period passively waiting. The left two bars are cells in standard medium without drug treatment. The middle two bars are cells subjected to cytochalasin D treatment. The right two bars are cells subjected to gerinstein treatment. (a) Percentage change in fit τ_F. (b) Percentage change in overall measurement of ΔG. (c) Percentage change in per-pixel measurement of ΔG.